Structural adjustments induced by heat treatment in ilvaite

PAOLA BONAZZI* AND LUCA BINDI

Dipartimento di Scienze della Terra, Università di Firenze, Via La Pira 4, I-50121, Florence, Italy

ABSTRACT

To verify the oxidation-dehydrogenation reaction induced by heat treatment of ilvaite in air, a crystal from Elba Island, Italy, was selected for annealing experiments and crystal chemical study. X-ray intensity data were collected and structure refinement was performed after each heat treatment (temperatures ranged from 400 to 700 °C). Oxidation of Fe^{2+} as well as loss of H atoms were deduced from examination of the structural changes occurring as the heating temperature was increased.

INTRODUCTION

Ilvaite is a mixed-valence Fe-bearing sorosilicate, typically occurring as a late forming mineral in Ca-Fe-Si skarn deposits (Burt 1971). Its chemical composition does not differ significantly from the ideal end-member, $Ca\ Fe_2^{2+}Fe^{3+}\ (Si_2O_7)O(OH)$, except for a considerable amount of Mn, mainly substituting for Fe^{2+} and, to a lesser extent, Ca (Carrozzini 1994); minor replacement of Fe^{2+} and Fe^{3+} by Mg and Al respectively were also observed (Naslund et al. 1983; Finger and Hazen 1987; Carrozzini 1994).

Ilvaite was considered to be orthorhombic (Belov and Mokeeva 1954; Beran and Bittner 1974; Haga and Takéuchi 1976), until Bartholomé et al. (1968) pointed out the existence of a monoclinic phase (space group $P2_1/a$). In the orthorhombic phase, Fe occupies two distinct octahedral positions: (1) the eightfold Wyckoff position $8d$ (labeled M1) and (2) the fourfold Wyckoff position $4c$ (labeled M2). The M1 site is randomly occupied by Fe^{2+} and Fe^{3+}, whereas M2 is completely filled by Fe^{2+} and Mn^{2+}, if any is present (Haga and Takéuchi 1976). At room temperature, ordering of Fe^{2+} and Fe^{3+} cations occurs, thus causing a small deviation from orthorhombic *Pnam* symmetry: as the mirror plane normal to the **c** axis is lost, the eightfold M1 site splits up into two independent crystallographic sites, M11 ($4e$) and M12 ($4e$), which mainly accommodate Fe^{2+} and Fe^{3+} respectively. This crystallographic phase transition occurs within the range 60–70 °C (Ghose et al. 1984a; Ghose et al. 1985; Robie et al. 1988). In the chemically pure synthetic ilvaite it occurs at 117 °C (Ghazi-Bayat et al. 1992).

Complete ordering between Fe^{2+} and Fe^{3+} should result in a β angle value of 90.45°, whereas complete disordering leads to β = 90.00° (Takéuchi et al. 1983). Ilvaites with β angle values ranging from 90.00° to ca. 90.35° are observed in nature (Takéuchi et al. 1993) and the degree of disorder is considered to vary accordingly. However, as Takéuchi et al. (1983) pointed out, different factors can combine to simulate disorder greater than actuality, such as polysynthetic twinning or $c/2$ displacement along the cation array of the octahedral chains. The value of the β angle is also affected by Mn content (Ghazi-Bayat et al. 1989). Intrinsically orthorhombic ilvaite may not exist in nature (Takéuchi et al. 1993). Variation of β angle or coexistence of different degrees of monoclinicity in the same crystal are apparently related to variation in mode and scale of twinnings incorporated with mainly inhomogeneous distribution of Mn (Takéuchi et al. 1994).

Several monoclinic structure refinements have been performed using both X-ray single crystal intensities (Finger et al. 1982; Takèuchi et al. 1983; Ghose et al. 1985; Finger and Hazen 1987; Ghose et al. 1989; Takéuchi et al. 1993; Carrozzini 1994; Takéuchi et al. 1994) and neutron powder diffraction data (Ghose et al. 1984b). Accurate structural data determined over a wide temperature range have been correlated with thermophysical, magnetic, and electrical properties (Yamanaka and Takéuchi 1979; Nolet and Burns 1979; Litterst and Amthauer 1984; Ghazi-Bayat et al. 1987; Robie et al. 1988; Xuemin et al. 1988; Ghazi-Bayat et al. 1989; Ghazi-Bayat et al. 1992). The role of pressure (Evans and Amthauer 1980; Finger and Hazen 1987; Ghazi-Bayat et al. 1993) as well as the effect of the $Mn^{2+} \leftrightarrow Fe^{2+}$ and $Al \leftrightarrow Fe^{3+}$ substitutions has been also examined (Ghazi-Bayat et al. 1989; Ghazi-Bayat et al. 1992; Amthauer et al. 1997). However, no structural data have been published concerning the behavior of ilvaite structure above 147 °C, except for the paper published by Robie et al. (1988), which measured the unit-cell dimensions of an ilvaite crystal within the temperature range 25–800 °C.

According to these authors, in this range, in addition to ordinary thermal expansion, three changes were observed: (1) monoclinic to orthorhombic phase at 70 °C; (2) orthorhombic to "*a substantially different orthorhombic phase*" at about 600 °C; (3) decomposition at about 750 °C. They also pointed out a dramatic change, not reversible in vacuum, near 430 °C, where *a* and *c* parameters deviate from their linear trend. This behavior, according to Robie et al. (1988), is probably related to a chemical reaction involving iron oxidation and hydrogen loss: $Ca\ Fe_2^{2+}Fe^{3+}(Si_2O_7)O(OH) \rightarrow Ca\ Fe^{2+}Fe_2^{3+}(Si_2O_7)O_2 + 1/2H_2$. This also accounts for the loss in weight (up to 0.5 wt%) ob-

served by Dietrich (1972) by thermo-gravimetric analysis. However, the oxidation-dehydrogenation process in mixed-valence metal minerals containing hydroxyl groups can easily take place without any dramatic change in topology other than minor structural adjustments. Structural variations accompanying oxidation-dehydrogenation were already studied in other minerals containing hydroxyls, such as amphiboles (Phillips et al. 1988; Phillips et al. 1989), or allanite and REE-bearing piemontite (Bonazzi and Menchetti 1994). The present work was undertaken to verify the occurrence in ilvaite of the oxidation-dehydrogenation reaction induced by heat treatment in air, and to examine the structural variations involved in this process.

Ghose (1988) suggested that natural orthorhombic ilvaites were most likely heated and either partially dehydrogenated or dehydroxylated subsequent to their formation. A knowledge of the crystal-chemical features of an oxy-ilvaite end-member should be very useful to evaluate a possible $Fe^{2+} + OH^- \rightarrow Fe^{3+} + O^{2-}$ substitutional mechanism in natural ilvaites, with regard to $p(O2)$-T conditions for the formation of iron-rich skarn deposits.

EXPERIMENTAL METHODS

A crystal of ilvaite (labeled RM) was selected for heat treatment and crystal-chemical study from a sample of Ca-Fe-Si skarn coming from Torre di Rio, Rio Marina, Elba Island, Italy (sample no. E-3819, Mineralogical Museum of the University of Florence).

Unit-cell parameters were determined by means of least-squares refinements using 25 reflections measured with a CAD4 single-crystal diffractometer.

Chemical composition was determined by means of electron microprobe JEOL JXA 8600 equipped with four wavelength dispersive spectrometers, operating at 15 kV and 10 nA. To check the homogeneity of the crystal, replicate analyses on different spots were performed. Table 1 reports the average chemical data and the atomic proportions calculated for the cation sum = 6.0. The crystal was subsequently removed from the resin and unit-cell parameters were determined again. Intensity data were collected in the θ-range 2–35°, using graphite-monochromatized Mo$K\alpha$ radiation, ω-scan mode, with scan speed of 4.1 °/min and scan width of 2.2°. Data were subsequently corrected for Lorentz-polarization and absorption effects (North et al. 1968).

The crystal was annealed in air for 48 h at selected temperatures ranging from 400 °C to 700 °C using a magnetic release furnace which allows rapid cooling to room temperature. After each heat treatment, determination of unit-cell parameters and intensity data collection was repeated using the same experimental conditions. As the annealing temperature increased, the crystal became brittle and minute fragments were lost. After the annealing at 720 °C reflections appeared broad and very weak, and the intensities were not collected.

Structure refinements were performed using the program SHELXL 93 (Sheldrick 1993). Although gradual changes in symmetry and systematic absences were consistent with the $P2_1/a \leftrightarrow Pnam$ transition, half an Ewald sphere was collected over the whole experiment, and least squares were preliminarily run assuming monoclinic symmetry. From the examination of results (see below), it was evident that the structure was substantially orthorhombic subsequent to the annealing at 500 °C.

Therefore, structure refinements were performed in the space group $Pnam$ except for structures at room temperature (RT), 400 and 450 °C. Details are given in Table 2. Fractional atomic coordinates and isotropic equivalent displacement parameters are given in Table 3.

DESCRIPTION OF THE STRUCTURE

The structure of ilvaite is based on octahedral ribbons linked together by Si_2O_7 groups and Ca-polyhedra. Hydrogen bonds, directed approximately along **a**, also concur to connect neighboring ribbons. These ribbons run parallel to **c** and consist of edge-sharing double chains of M11 and M12 octahedra with the larger M2 octahedron alternatively attached above and below by means of four shared edges (Fig. 1).

When M11 and M12 are equivalent, the (O3-O7)$_{M11}$ edge equals the (O3-O7)$_{M12}$ edge, so that the direction of the chains (**c** axis), as defined by the (O3-O7)$_{M11}$-(O3-O7)$_{M12}$ zigzag line, is normal to **a** (Takéuchi et al. 1983). As Fe ordering increases,

TABLE 1. Chemical composition (wt%) and atomic proportions of the crystal RM

SiO_2	30.21	Si^{4+}	2.02
Fe_2O_3	19.07	Fe^{3+}	0.96
Al_2O_3	0.45	Al^{3+}	0.04
FeO	34.32	Fe^{2+}	1.92
CaO	13.66	Ca^{2+}	0.98
MnO	0.84	Mn^{2+}	0.05
MgO	0.27	Mg^{2+}	0.03
Total	98.82	Σ cations	6.00

Note: Fe determined as FeO and subsequently distributed between FeO and Fe_2O_3 according to the criterion ($Fe^{3+} + Al^{3+}$) = 1 atom per formula unit. H_2O was not determined.

TABLE 2. Unit-cell parameters determined after each heat treatment and structure refinement details

	RM-RT	RM-400	RM-450	RM-500	RM-550	RM-600	RM-615	RM-625	RM-660	RM-675	RM-700
a(Å)	13.006(1)	13.015(1)	13.014 (1)	13.005(1)	13.013(1)	13.015(1)	13.012(2)	13.007(2)	13.008(2)	13.013(2)	13.006(4)
b(Å)	8.808(1)	8.803(1)	8.807(1)	8.800(1)	8.802(1)	8.802(1)	8.801(2)	8.805(2)	8.802(2)	8.804(1)	8.804(2)
c(Å)	5.850(1)	5.842(1)	5.846(1)	5.847(1)	5.849(1)	5.847(1)	5.850(1)	5.844(1)	5.842(1)	5.841(1)	5.836(2)
β (°)	90.34(1)	90.16(1)	90.10(1)	90.00	90.00	90.00	90.00	90.00	90.00	90.00	90.00
V(Å^3)	670.1(2)	669.4(3)	670.0(3)	669.2(2)	669.9(2)	669.7(3)	669.9(2)	669.3(3)	668.8(2)	669.2(2)	668.3(3)
Sp. Grp.	$P2_1/a$	$P2_1/a$	$P2_1/a$	$Pnam$	$Pnam$	$Pnam$	$Pnam$	$Pnam$	$Pnam$	$Pnam$	$Pnam$
n.coll.refl.	6352	6348	6224	6342	6328	6356	6353	6340	6336	6355	6332
n.ind.refl.	2941	2941	2903	1589	1589	1592	1589	1587	1585	1585	1587
n.obs.refl.	2604	2618	2592	1473	1467	1497	1485	1488	1469	1528	1497
n.ref.par.	144	144	144	89	89	89	89	86	86	86	86
R_{symm} (%)	2.98	2.94	3.11	3.04	2.66	2.58	2.47	2.73	2.08	1.70	2.50
R_{all} (%)	3.06	3.59	3.55	2.96	2.88	3.73	3.38	3.67	3.19	3.44	3.61
R_{obs} (%)	2.50	2.99	2.90	2.57	2.55	3.46	3.08	4.00	3.56	3.30	3.35

(O3-O7)$_{M11}$ and (O3-O7)$_{M12}$ become different in length, and the zigzag line becomes oblique to **a**. Before heating, the crystal RM shows a structural arrangement very similar to that found for other monoclinic natural ilvaites (Takéuchi et al. 1983; Ghose et al. 1984b; Finger and Hazen 1987; Carrozzini 1994; Takéuchi et al. 1994). In silicate minerals, values of 2.135 Å and 2.025 Å can be considered for <Fe^{2+}-O> and <Fe^{3+}-O> respectively (Ghose 1969). These values can be used to estimate the Fe^{2+}-Fe^{3+} distribution between the M11 and M12 sites in ilvaite. The mean value of 2.080 Å matches the <M1-O> distance in the orthorhombic ilvaite (2.081 Å, according to Beran and Bittner 1974) and agrees perfectly with the value of the grand mean <M11,12-O> in RM crystal before oxidation takes place. In the untreated crystal (RM-RT) <M11-O> = 2.110 Å and <M12-O> = 2.049 Å corresponding to M11 = 0.78 Fe^{2+} + 0.22 Fe^{3+} and M12 = 0.78 Fe^{3+} + 0.22 Fe^{2+}. The resulting order parameter Q = 0.54 barely agrees with that predicted (0.68) as function of the β angle value on the basis of the relation proposed by Carrozzini (1994). The very low content of Mg and Al, which probably enters the M11 (n.e$^-$ = 25.4) and the M12 (n.e$^-$ = 25.4) sites respectively, should not significantly affect
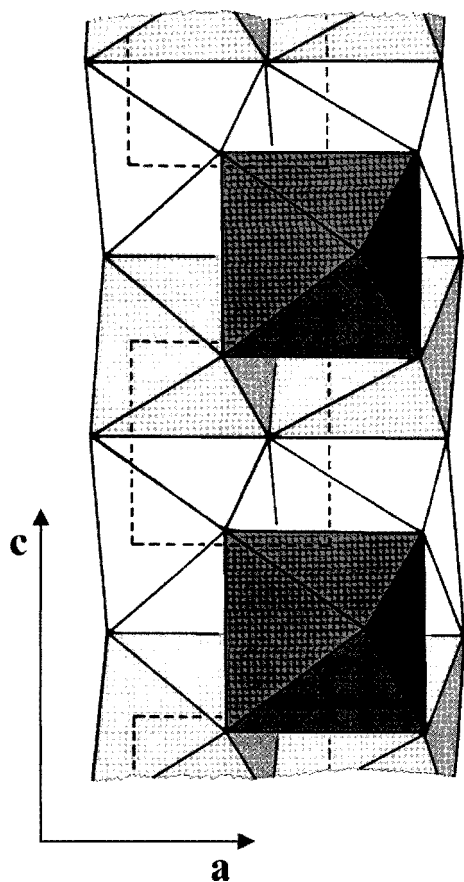

FIGURE 1. The double octahedral chain in the structure of ilvaite. White, light gray, and dark gray polyhedra represent M11, M12, and M2, respectively. Dashed squares represent the M2 octahedra attached below the octahedral chain.

TABLE 3a. Fractional atomic coordinates and equivalent isotropic displacement parameters

		RM-RT	RM-400	RM-450
Ca	x/a	0.81285(2)	0.81287(2)	0.81287(3)
	y/b	0.37021(4)	0.37024(3)	0.37029(4)
	z/c	0.75327(6)	0.75082(6)	0.75072(7)
	U_{eq}	0.00855(8)	0.01025(9)	0.00958(8)
M11	x/a	0.89018(2)	0.89008(2)	0.89007(2)
	y/b	0.04961(3)	0.05063(3)	0.05073(3)
	z/c	0.00734(4)	0.00746(3)	0.00734(5)
	U_{eq}	0.00736(8)	0.00869(10)	0.00807(9)
M12	x/a	0.88999(2)	0.89002(2)	0.89000(2)
	y/b	0.05200(3)	0.05112(3)	0.05119(3)
	z/c	0.49267(4)	0.49256(5)	0.49276(5)
	U_{eq}	0.00662(8)	0.00844(10)	0.00799(9)
M2	x/a	0.94076(2)	0.94072(2)	0.94063(2)
	y/b	0.74006(3)	0.74001(3)	0.74003(3)
	z/c	0.24863(5)	0.24967(6)	0.24975(5)
	U_{eq}	0.00770(7)	0.00910(9)	0.00857(8)
Si1	x/a	0.95950(3)	0.95950(3)	0.95958(4)
	y/b	0.36859(5)	0.36867(6)	0.36863(6)
	z/c	0.24924(8)	0.24978(8)	0.24986(10)
	U_{eq}	0.00589(9)	0.00756(11)	0.00688(10)
Si2	x/a	0.67948(3)	0.67940(3)	0.67950(4)
	y/b	0.22718(5)	0.22725(6)	0.22731(6)
	z/c	0.25216(8)	0.25048(8)	0.25047(10)
	U_{eq}	0.00601(9)	0.00770(11)	0.00689(10)
O1	x/a	0.00992(10)	0.00972(10)	0.00985(11)
	y/b	0.02941(14)	0.02937(14)	0.02910(16)
	z/c	0.73668(23)	0.74624(23)	0.74651(29)
	U_{eq}	0.01007(22)	0.01339(28)	0.01293(27)
O21	x/a	0.93723(10)	0.93673(10)	0.93651(11)
	y/b	0.27240(14)	0.27236(16)	0.27249(16)
	z/c	0.01584(22)	0.01684(27)	0.01682(25)
	U_{eq}	0.00851(20)	0.00988(24)	0.00920(24)
O22	x/a	0.93527(10)	0.93618(10)	0.93628(11)
	y/b	0.27256(14)	0.27256(17)	0.27240(16)
	z/c	0.48251(22)	0.48296(22)	0.48262(25)
	U_{eq}	0.00822(20)	0.01017(25)	0.00913(23)
O3	x/a	0.77743(9)	0.77741(11)	0.77748(11)
	y/b	0.10907(14)	0.10954(17)	0.10944(16)
	z/c	0.25657(22)	0.25153(28)	0.25130(26)
	U_{eq}	0.00817(20)	0.01054(26)	0.00967(25)
O41	x/a	0.67131(9)	0.67091(11)	0.67102(11)
	y/b	0.32760(13)	0.32943(17)	0.32928(15)
	z/c	0.01900(22)	0.01879(26)	0.01863(25)
	U_{eq}	0.00836(20)	0.01017(25)	0.00942(24)
O42	x/a	0.67037(9)	0.67071(9)	0.67084(11)
	y/b	0.33147(13)	0.33023(16)	0.33013(15)
	z/c	0.48218(21)	0.48127(27)	0.48177(25)
	U_{eq}	0.00786(20)	0.01023(25)	0.00935(24)
O5	x/a	0.58487(9)	0.58492(11)	0.58485(11)
	y/b	0.10063(14)	0.10079(16)	0.10108(15)
	z/c	0.25333(22)	0.25082(26)	0.25056(26)
	U_{eq}	0.00816(20)	0.00920(24)	0.00907(23)
O6	x/a	0.60183(10)	0.60185(12)	0.60163(11)
	y/b	0.02559(14)	0.02546(17)	0.02554(16)
	z/c	0.75255(25)	0.75058(30)	0.75061(29)
	U_{eq}	0.01070(22)	0.01232(27)	0.01173(26)
O7	x/a	0.79796(10)	0.79802(12)	0.79821(11)
	y/b	0.10924(14)	0.10917(17)	0.10931(16)
	z/c	0.74425(22)	0.74867(27)	0.74935(26)
	U_{eq}	0.00849(20)	0.01041(25)	0.00948(24)
H	x/a	0.7381(30)	0.7368(34)	0.7394(35)
	y/b	0.0770(44)	0.0734(50)	0.0789(51)
	z/c	0.7381(69)	0.7501(79)	0.7417(86)
	U_{iso}	0.036(10)	0.034(11)	0.047(13)

Note: e.s.d.'s (in parentheses).

TABLE 3b. Fractional atomic coordinates and equivalent isotropic displacement parameters

		RM-500	RM-550	RM-600	RM-615	RM-625	RM-660	RM-675	RM-700
Ca	x/a	0.81303(4)	0.81328(4)	0.81393(6)	0.81437(5)	0.81461(6)	0.81562(5)	0.81593(5)	0.81636(5)
	y/b	0.37050(5)	0.37080(6)	0.37154(8)	0.37215(7)	0.37226(9)	0.37326(7)	0.37354(8)	0.37376(8)
	z/c	0.75000	0.75000	0.75000	0.75000	0.75000	0.75000	0.75000	0.75000
	U_{eq}	0.00956(11)	0.00891(11)	0.00945(16)	0.00880(13)	0.00996(17)	0.00957(14)	0.01083(15)	0.01285(15)
M1	x/a	0.88996(2)	0.88981(2)	0.88955(3)	0.88933(2)	0.88925(3)	0.88880(3)	0.88868(3)	0.88856(3)
	y/b	0.05113(3)	0.05150(3)	0.05225(4)	0.05276(4)	0.05298(5)	0.05419(4)	0.05457(4)	0.05505(4)
	z/c	0.00695(4)	0.00594(5)	0.00369(7)	0.00182(6)	0.00143(8)	-0.00169(7)	-0.00250(7)	-0.00357(7)
	U_{eq}	0.00802(8)	0.00758(8)	0.00790(11)	0.00750(9)	0.00840(12)	0.00773(10)	0.00878(11)	0.01016(11)
M2	x/a	0.94045(3)	0.93991(3)	0.93864(4)	0.93779(4)	0.93739(5)	0.93565(4)	0.93508(4)	0.93421(4)
	y/b	0.73995(4)	0.73990(4)	0.73969(6)	0.73957(5)	0.73945(7)	0.73917(6)	0.73909(6)	0.73921(6)
	z/c	0.25000	0.25000	0.25000	0.25000	0.25000	0.25000	0.25000	0.25000
	U_{eq}	0.00853(10)	0.00791(10)	0.00819(15)	0.00779(12)	0.00859(16)	0.00830(13)	0.00950(14)	0.01120(15)
Si1	x/a	0.95973(5)	0.96007(5)	0.96097(8)	0.96151(7)	0.96180(9)	0.96320(7)	0.96364(7)	0.96437(8)
	y/b	0.36848(7)	0.36831(8)	0.36795(11)	0.36769(10)	0.36767(12)	0.36724(10)	0.36719(11)	0.36704(11)
	z/c	0.25000	0.25000	0.25000	0.25000	0.25000	0.25000	0.25000	0.25000
	U_{eq}	0.00683(13)	0.00600(13)	0.00618(19)	0.00573(16)	0.00661(20)	0.00639(16)	0.00757(17)	0.00966(18)
Si2	x/a	0.67954(5)	0.67993(5)	0.68078(8)	0.68148(7)	0.68167(8)	0.68289(7)	0.68322(7)	0.68385(7)
	y/b	0.22764(7)	0.22798(8)	0.22868(11)	0.22939(9)	0.22961(12)	0.23103(10)	0.23152(11)	0.23199(10)
	z/c	0.25000	0.25000	0.25000	0.25000	0.25000	0.25000	0.25000	0.25000
	U_{eq}	0.00685(13)	0.00632(13)	0.00629(19)	0.00576(16)	0.00658(20)	0.00589(16)	0.00695(17)	0.00801(17)
O1	x/a	0.01009(14)	0.01067(15)	0.01197(23)	0.01277(20)	0.01293(25)	0.01464(19)	0.01507(21)	0.01573(21)
	y/b	0.02908(21)	0.02862(21)	0.02755(32)	0.02720(27)	0.02673(35)	0.02588(28)	0.02534(30)	0.02467(30)
	z/c	0.75000	0.75000	0.75000	0.75000	0.75000	0.75000	0.75000	0.75000
	U_{eq}	0.01288(34)	0.01195(36)	0.01270(53)	0.01215(45)	0.01315(58)	0.01118(45)	0.01265(48)	0.01451(48)
O2	x/a	0.93650(9)	0.93683(10)	0.93765(14)	0.93804(13)	0.93843(15)	0.93945(13)	0.93994(14)	0.94065(14)
	y/b	0.27246(14)	0.27212(14)	0.27167(20)	0.27138(17)	0.27132(22)	0.27077(18)	0.27073(20)	0.27065(20)
	z/c	0.01687(21)	0.01684(23)	0.01674(34)	0.01656(28)	0.01651(37)	0.01623(30)	0.01641(32)	0.01616(31)
	U_{eq}	0.00907(21)	0.00854(22)	0.00887(32)	0.00855(27)	0.00963(35)	0.00937(28)	0.01065(31)	0.01267(31)
O3	x/a	0.77766(13)	0.77793(14)	0.77888(21)	0.77963(18)	0.77989(23)	0.78146(18)	0.78199(20)	0.78262(20)
	y/b	0.10957(21)	0.10975(22)	0.11065(22)	0.11118(26)	0.11128(34)	0.11217(28)	0.11239(29)	0.11255(30)
	z/c	0.25000	0.25000	0.25000	0.25000	0.25000	0.25000	0.25000	0.25000
	U_{eq}	0.00910(30)	0.00858(32)	0.00821(46)	0.00752(38)	0.00862(49)	0.00818(40)	0.00939(42)	0.01139(43)
O4	x/a	0.67089(9)	0.67116(9)	0.67178(14)	0.67208(12)	0.67217(15)	0.67292(12)	0.67321(14)	0.67356(14)
	y/b	0.33005(13)	0.33030(14)	0.33119(20)	0.33193(17)	0.33186(22)	0.33335(18)	0.33364(20)	0.33367(20)
	z/c	0.01854(22)	0.01831(23)	0.01805(34)	0.01836(29)	0.01774(38)	0.01754(30)	0.01744(32)	0.01641(32)
	U_{eq}	0.00920(22)	0.00839(23)	0.00882(33)	0.00826(27)	0.00924(35)	0.00901(29)	0.01038(31)	0.01305(32)
O5	x/a	0.58510(13)	0.58548(14)	0.58608(20)	0.58682(18)	0.58696(23)	0.58862(19)	0.58908(20)	0.58968(21)
	y/b	0.10122(20)	0.10167(21)	0.10232(31)	0.10303(26)	0.10293(34)	0.10440(28)	0.10482(30)	0.10488(30)
	z/c	0.25000	0.25000	0.25000	0.25000	0.25000	0.25000	0.25000	0.25000
	U_{eq}	0.00884(29)	0.00779(31)	0.00848(45)	0.00818(38)	0.00962(50)	0.00950(41)	0.01108(44)	0.01315(45)
O6	x/a	0.60152(14)	0.60102(15)	0.60011(23)	0.59924(21)	0.59906(26)	0.59678(22)	0.59638(24)	0.59543(24)
	y/b	0.02558(21)	0.02553(21)	0.02480(32)	0.02467(27)	0.02465(36)	0.02416(29)	0.02413(32)	0.02378(32)
	z/c	0.75000	0.75000	0.75000	0.75000	0.75000	0.75000	0.75000	0.75000
	U_{eq}	0.01173(32)	0.01138(35)	0.01257(52)	0.01283(45)	0.01432(59)	0.01465(49)	0.01602(52)	0.01897(54)
O7	x/a	0.79861(14)	0.79899(15)	0.80060(24)	0.80151(21)	0.80173(26)	0.80392(21)	0.80464(22)	0.80613(22)
	y/b	0.10947(21)	0.10990(22)	0.11071(33)	0.11156(28)	0.11110(35)	0.11225(28)	0.11229(30)	0.11229(30)
	z/c	0.75000	0.75000	0.75000	0.75000	0.75000	0.75000	0.75000	0.75000
	U_{eq}	0.00965(30)	0.00954(33)	0.01066(49)	0.01056(42)	0.01189(54)	0.01128(44)	0.01247(47)	0.01357(46)
H	x/a	0.7420(55)	0.7438(75)	0.7611(84)	0.7629(79)				
	y/b	0.0727(72)	0.0535(10)	0.0717(112)	0.0549(102)				
	z/c	0.75000	0.75000	0.75000	0.75000				
	U_{iso}	0.062(23)	0.196(35)	0.088(36)	0.115(34)				

Note: e.s.d.'s (in parentheses).

TABLE 4a. Structural parameters for RM crystal (monoclinic symmetry)

		RM-RT	RM-400	RM-450
Ca -	O21	2.385(1)	2.396(2)	2.396(1)
	O22	2.411(1)	2.404(2)	2.406(2)
	O3	2.410(1)	2.412(2)	2.412(1)
	O41	2.445(1)	2.451(2)	2.450(2)
	O42	2.456(1)	2.452(2)	2.450(1)
	O5	2.427(1)	2.427(1)	2.430(1)
	O7	2.307(1)	2.306(2)	2.306(1)
	mean	2.406	2.407	2.407
M11 -	O1	2.096(1)	2.063(2)	2.063(2)
	O1'	2.235(1)	2.191(2)	2.191(2)
	O21	2.056(1)	2.045(1)	2.045(1)
	O3	2.139(1)	2.113(2)	2.111(2)
	O41	2.118(1)	2.108(1)	2.111(1)
	O7	2.015(1)	1.994(2)	1.991(1)
	mean	2.110	2.086	2.085
	λ	1.0077	1.0068	1.0068
	σ^2	20.95	18.94	18.64
M12 -	O1	2.007(1)	2.040(2)	2.040(2)
	O1'	2.118(1)	2.156(2)	2.159(2)
	O22	2.031(1)	2.041(2)	2.040(1)
	O3	2.069(1)	2.094(2)	2.096(1)
	O42	2.101(1)	2.105(1)	2.107(1)
	O7	1.968(1)	1.986(2)	1.986(2)
	mean	2.049	2.070	2.072
	λ	1.0072	1.0066	1.0066
	σ^2	21.13	19.12	18.77
M2 -	O1	2.131(1)	2.130(2)	2.133(1)
	O21	2.226(1)	2.235(2)	2.237(2)
	O22	2.248(1)	2.237(2)	2.240(1)
	O41	2.268(1)	2.275(2)	2.277(1)
	O42	2.290(1)	2.284(2)	2.282(2)
	O6	1.969(1)	1.968(2)	1.967(1)
	mean	2.189	2.188	2.189
	λ	1.0212	1.0210	1.0210
	σ^2	58.95	58.36	58.22
Si1 -	O21	1.631(1)	1.630(2)	1.631(2)
	O22	1.638(1)	1.633(2)	1.632(2)
	O5	1.653(1)	1.654(2)	1.652(1)
	O6	1.596(1)	1.595(2)	1.595(2)
	mean	1.630	1.628	1.628
	λ	1.0026	1.0027	1.0026
	σ^2	10.17	10.47	10.29
Si2 -	O3	1.645(1)	1.643(2)	1.644(1)
	O41	1.629(1)	1.629(2)	1.629(2)
	O42	1.632(1)	1.629(2)	1.631(2)
	O5	1.660(1)	1.659(2)	1.659(1)
	mean	1.642	1.640	1.641
	λ	1.0086	1.0083	1.0083
	σ^2	32.96	31.88	31.89
O7 -	O6	2.656(1)	2.657(2)	2.663(2)

Note: Distances are reported in Å; the mean quadratic elongation (λ) and the angle variance (σ^2) were computed according to Robinson et al. (1971).

FIGURE 2. The mean <M1-O> distance plotted against the heating temperature.

leads to a mean electron number close to 20.0 within the estimated standard deviation, thus excluding any Ca-Mn^{2+} substitution. Both tetrahedra and Ca-polyhedron do not show any marked variation with increasing heating temperature. The following discussion, therefore, will mainly deal with octahedral framework and hydrogen bonding system. Bond distances and distortion parameters are given in Table 4; list of atomic fractional coordinates and anisotropic thermal displacements are available from the authors.

DISCUSSION

Symmetry

The monoclinic structure of ilvaite only deviates slightly from orthorhombic symmetry. The strong pseudosymmetry between pairs of independent 4e positions (M11/M12, O12/O22, O41/O42) causes topology to be nearly consistent with *Pnam* space group. The 0*kl* reflections with $k + l = 2n + 1$ were very weak even in the untreated crystal with $\beta = 90.34°$. The only observed 0*kl* reflections (i.e., 021, 041, 061, 072, 003, 023, and 043) show <Fo/σ(Fo)> ratio close to 9.0 for RM-RT, near to 6.0 for RM-400 and RM-450 and approaches 3.0 after heating at 500 °C. At this point the β angle was found to be 90.00° within the limits of experimental error, and details of the structure, obtained by refinement in the monoclinic space group ($R = 2.83\%$), were consistent with the orthorhombic symmetry ($R = 2.57\%$). However, it should be kept in mind that an apparent orthorhombic symmetry can be easily simulated by the co-existence of fine components polysynthetically twinned on both (001) and (100) (Takéuchi et al. 1994). Such a twinning would be easily generated if mistakes in the cation array take place during the Fe^{2+}-Fe^{3+} ordering process which occurs when the crystal is cooled through the phase transition temperature.

the observed bond distances.

As expected, M2 is the largest and most irregular octahedral site in the structure. According to the model proposed by Carrozzini (1994), the observed <M2-O> distance (2.189 Å) is consistent with a content of Mn^{2+} replacing Fe^{2+} of 0.06 apfu, which agrees perfectly with the value determined by chemical analysis. The <Si1-O> and <Si2-O> distances (1.630 and 1.642 Å respectively) are consistent with the assumption that no cation substitution affects the tetrahedral sites. As expected for a Mn-poor ilvaite, the refinement of occupancy at the Ca-site
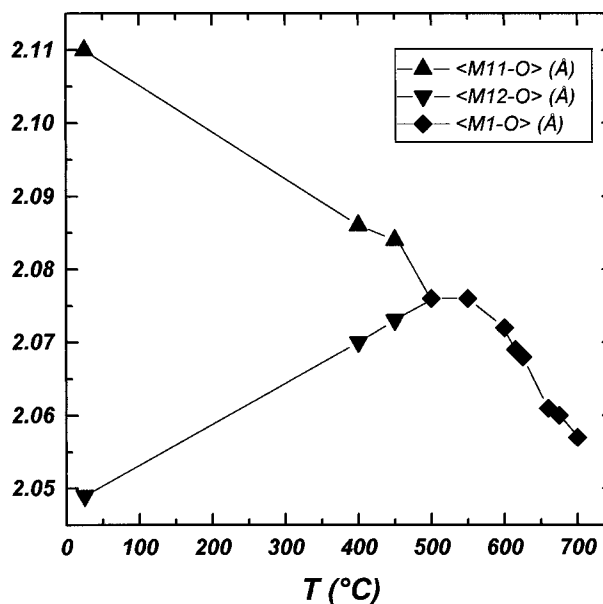
TABLE 4b. Structure parameters for RM crystal (orthorhombic symmetry)

		RM-500	RM-550	RM-600	RM-615	RM-625	RM-660	RM-675	RM-700
Ca -	O2(×2)	2.399(1)	2.403(1)	2.408(2)	2.410(2)	2.410(2)	2.414(2)	2.418(2)	2.419(2)
	O3	2.412(2)	2.415(2)	2.427(3)	2.433(2)	2.437(3)	2.453(3)	2.459(3)	2.465(3)
	O4(×2)	2.451(1)	2.452(1)	2.451(2)	2.453(2)	2.451(2)	2.452(2)	2.452(2)	2.448(2)
	O5	2.424(2)	2.422(2)	2.412(3)	2.405(2)	2.401(3)	2.386(3)	2.382(3)	2.374(3)
	O7	2.305(2)	2.304(2)	2.302(3)	2.300(2)	2.306(3)	2.302(3)	2.305(3)	2.306(3)
	Mean	2.406	2.407	2.408	2.409	2.410	2.410	2.412	2.411
M1 -	O1	2.051(1)	2.052(1)	2.052(2)	2.056(2)	2.055(2)	2.058(2)	2.059(2)	2.057(2)
	O1'	2.176(1)	2.181(1)	2.188(2)	2.191(2)	2.191(2)	2.201(2)	2.205(2)	2.208(2)
	O2	2.040(1)	2.037(1)	2.032(2)	2.028(2)	2.028(2)	2.020(2)	2.020(2)	2.019(2)
	O3	2.102(1)	2.102(1)	2.101(2)	2.100(2)	2.097(2)	2.091(2)	2.089(2)	2.084(2)
	O4	2.106(1)	2.107(1)	2.107(2)	2.105(2)	2.107(2)	2.105(2)	2.107(2)	2.111(2)
	O7	1.983(1)	1.975(1)	1.951(2)	1.935(2)	1.928(2)	1.893(2)	1.883(2)	1.863(2)
	Mean	2.076	2.076	2.072	2.069	2.068	2.061	2.060	2.057
	λ	1.0067	1.0066	1.0068	1.0070	1.0070	1.0080	1.0083	1.0090
	σ^2	18.52	17.72	16.66	16.40	16.07	16.61	16.66	17.45
M2 -	O1	2.132(2)	2.137(2)	2.147(3)	2.151(2)	2.158(3)	2.167(3)	2.173(3)	2.178(3)
	O2(×2)	2.238(1)	2.241(1)	2.244(2)	2.248(2)	2.246(2)	2.251(2)	2.253(2)	2.252(2)
	O4(×2)	2.278(1)	2.277(1)	2.274(2)	2.274(2)	2.267(2)	2.264(2)	2.263(2)	2.252(2)
	O6	1.964(2)	1.961(2)	1.958(3)	1.952(3)	1.950(3)	1.939(3)	1.936(3)	1.935(3)
	Mean	2.188	2.189	2.190	2.191	2.189	2.189	2.190	2.187
	λ	1.0212	1.0217	1.0226	1.0236	1.0237	1.0259	1.0263	1.0267
	σ^2	58.90	60.25	63.85	66.71	67.80	74.93	76.63	78.69
Si1 -	O2(×2)	1.632(1)	1.633(1)	1.634(2)	1.636(2)	1.635(2)	1.638(2)	1.636(2)	1.636(2)
	O5	1.652(2)	1.653(2)	1.649(3)	1.651(2)	1.648(3)	1.650(3)	1.651(3)	1.648(3)
	O6	1.596(2)	1.596(2)	1.593(3)	1.592(3)	1.593(3)	1.586(3)	1.587(3)	1.584(3)
	Mean	1.628	1.629	1.628	1.629	1.628	1.628	1.628	1.626
	λ	1.0027	1.0027	1.0027	1.0027	1.0027	1.0028	1.0028	1.0028
	σ^2	10.47	10.56	10.49	10.61	10.61	10.57	10.82	10.76
Si2 -	O3	1.646(2)	1.646(2)	1.646(3)	1.647(2)	1.649(3)	1.655(3)	1.659(3)	1.660(3)
	O4(×2)	1.630(1)	1.631(1)	1.633(2)	1.633(2)	1.633(2)	1.635(2)	1.634(2)	1.636(2)
	O5	1.657(2)	1.657(2)	1.660(3)	1.659(2)	1.662(3)	1.657(3)	1.657(3)	1.659(3)
	Mean	1.641	1.641	1.643	1.643	1.644	1.645	1.646	1.648
	λ	1.0084	1.0086	1.0085	1.0087	1.0089	1.0093	1.0094	1.0099
	σ^2	32.44	32.84	32.41	33.26	33.98	35.24	35.57	37.12
O7 -	O6	2.667(2)	2.681(2)	2.717(3)	2.741(3)	2.744(3)	2.804(3)	2.819(3)	2.849(3)

Note: Distances are reported in Å; the mean quadratic elongation (λ) and the angle variance (σ^2) were computed according to Robinson et al. (1971).
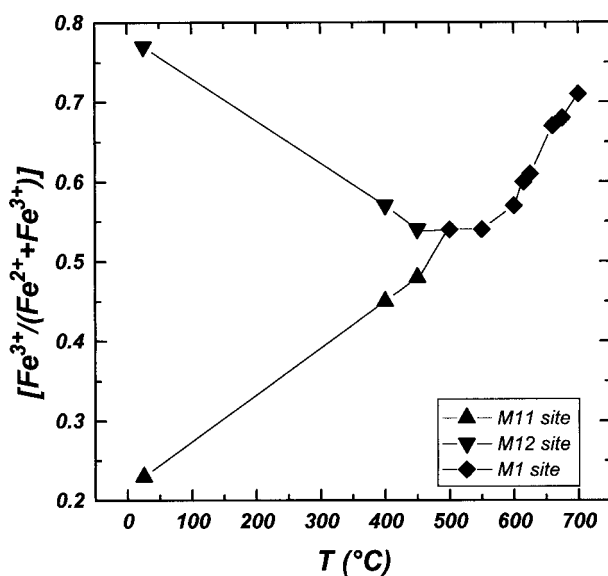

FIGURE 3. The [Fe^{3+}/(Fe^{2+} + Fe^{3+})] ratio in the M1 site plotted against the heating temperature.
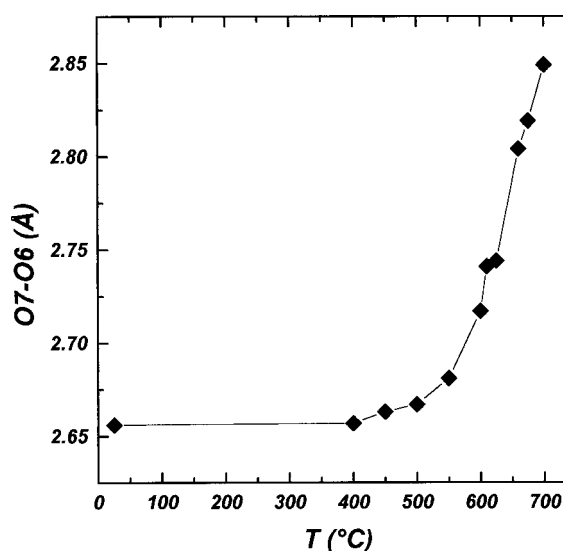

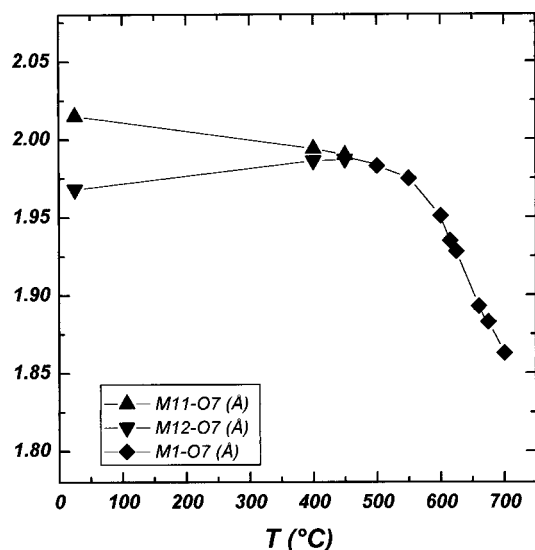FIGURE 4. The donor-acceptor distance (O7-O6) plotted against the heating temperature.

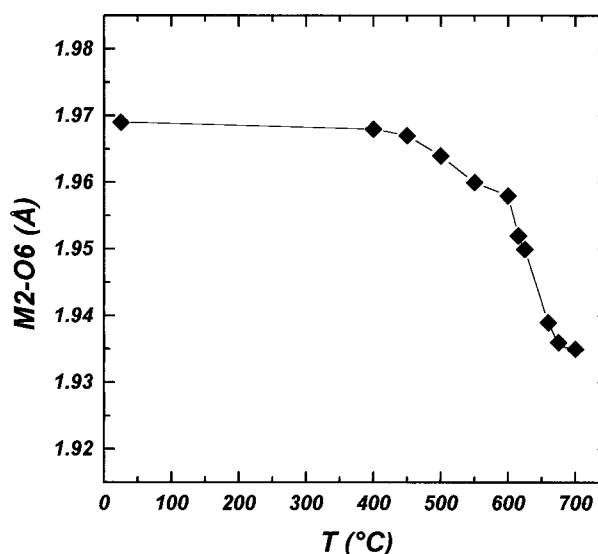**FIGURE 5.** The M1-O7 distance plotted against the heating temperature.

FIGURE 6. M2-O6 distance plotted against the heating temperature.

Iron distribution

In the untreated crystal an ordered distribution of Fe^{2+} and Fe^{3+} between M11 and M12 can be observed. As the heating temperature increases, the apparent disordering between M11 and M12 sites becomes significant: it is made evident from the mean <M11-O> and <M12-O> distances which gradually converge to a common value of 2.076 Å (Fig. 2). After the heat

treatment at 500 °C, the high-temperature Fe^{2+}-Fe^{3+} distribution between M11 and M12 apparently persists even after cooling to room temperature. This feature, as discussed above, is probably related to the presence of twinned ordered domains.

Effect of iron oxidation

The grand mean <M11,M12-O> decreases slightly up to 550 °C (from 2.080 in RM-RT to 2.076 Å in RM-550). After this point, the <M1-O> distance decreases with a linear trend down to 2.057 Å in RM-700. Taking into account the values published by Ghose (1969), the M1 site population was estimated for each step: as shown in Fig. 3, the strong increase of the $[Fe^{3+}/(Fe^{2+} + Fe^{3+})]_{M1}$ ratio takes place after the 550 °C heat treatment. With the increase of the Fe^{3+} content, the M1-octahedron becomes slightly more regular (σ^2_{M1} ranging from 18.52 for RM-500 to 17.45 for RM-700). On the contrary, the large M2-octahedron, which shares four edges with four M1-octahedra, becomes more irregular (σ^2_{M2} ranging from 58.90 for RM-500 to 78.69 for RM-700) because of the decrease of the M1-volume. The volume contraction due to the oxidation, in fact, only affects the iron at the M1 site, whereas the M2 octahedron does not change in size significantly over whole the temperature range.

TABLE 5a. Empirical bond-valence balance for RM-RT

	Ca	M11	M12	M2	Si1	Si2	H	
O1		0.377	0.516					
O1				0.371				1.91
O1		0.260	0.382					
O21	0.300	0.420		0.287	0.994			2.00
O22	0.280			0.484	0.271	0.976		2.01
O3	0.280	0.336	0.438			0.990		2.04
O41	0.255	0.357		0.257		1.034		1.90
O42	0.247		0.390	0.241		1.025		1.90
O5	0.268				0.937	0.951		2.16
O6				0.575	1.093		0.333	2.00
O7	0.370	0.471	0.573				0.667	2.08
	2.00	2.22	2.78	2.00	4.00	4.00	1.00	18.00

Note: Bond valences are weighted assuming M11= $0.75Fe^{2+}$ + $0.22Fe^{3+}$ + 0.03Mg; M12 = $0.74Fe^{3+}$ + $0.22Fe^{2+}$ + 0.04Al; M2 = $0.95Fe^{2+}$ + $0.05Mn^{2+}$. The empirical parameters used in the calculations are those of Brown and Altermatt (1985).

TABLE 5b. Empirical bond-valence balance for RM-700

	Ca	M1	M2	Si1	Si2	H	
O1		0.432 ×2					
O1			0.322				1.76
O1		0.287 ×2					
O2	0.277*	0.478 ×2	0.264 ×2	0.971 ×2			1.99 ×2
O3	0.245	0.401 ×2			0.967		2.01
O4	0.256*	0.373 ×2	0.264 ×2		1.032 ×2		1.93 ×2
O5	0.313			0.940	0.970		2.22
O6			0.622	1.118		0.20	1.74
O7	0.376	0.729 ×2				0.40	1.83
	2.00	2.70 ×2	2.00	4.00	4.00	0.60	18.00

Note: Bond valences are weighted assuming M1 = $0.66Fe^{3+}$ + $0.27Fe^{2+}$ + 0.03Mg + 0.04Al; M2 = $0.95Fe^{2+}$ + $0.05Mn^{2+}$. The empirical parameters used in the calculations are those of Brown and Altermatt (1985).
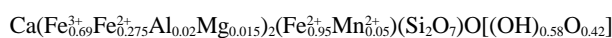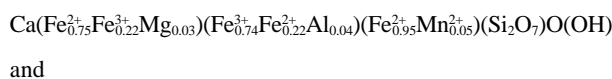
Effect of dehydrogenation

The most pronounced evidence of the hydrogen loss accompanying the oxidation reaction is the lengthening of the donor (O7)-acceptor (O6) distance (Fig. 4), which increases markedly after the annealing at 550 °C (from 2.667 Å in RM-500 to 2.849 Å in RM-700). Minor but significant variations of O7-O6 interdistance are observed even before (see Table 4a), thus suggesting that the corresponding small variation in the <M11,12-O> distance is significant as well. The loss of positive charge on the oxygen O7 due to partial dehydrogenation is directly compensated by the oxidation of divalent iron at M1. Among the octahedral distances, M1-O7 is the most sensitive to the ongoing oxidation-dehydrogenation process (Fig. 5). On the other hand, Ca-O7, that is the shortest bond distances within the Ca-polyhedron, does not change significantly by heating. The acceptor oxygen (O6), which links Si1 and M2, approaches M2 (Fig. 6) to balance the partial loss of hydrogen. Table 5 reports the charge balance computed according to Brown and Altermatt (1985) for RM-RT and RM-700, respectively.

CONCLUSIONS

The oxidation-dehydrogenation reaction produced by heating natural ilvaite in air begins to develop at 500–550 °C. No phase transition was observed over the whole temperature range: therefore the structure of ilvaite can easily lose hydrogen without any change in topology and/or in symmetry. The structure responds to Fe^{2+} oxidation with adjustments involving bond distances and angles inside the double octahedral chain. The loss of hydrogen, estimated to be about 40% after the 700 °C heat treatment, causes variations in the connection between adjacent chains due to the weakening of hydrogen bond.

On the basis of chemical and structural results and keeping in mind crystal-chemical relationships in ilvaite, the following crystal-chemical formula can be assigned:

$$Ca(Fe^{2+}_{0.75}Fe^{3+}_{0.22}Mg_{0.03})(Fe^{3+}_{0.74}Fe^{2+}_{0.22}Al_{0.04})(Fe^{2+}_{0.95}Mn^{2+}_{0.05})(Si_2O_7)O(OH)$$

and

$$Ca(Fe^{3+}_{0.69}Fe^{2+}_{0.275}Al_{0.02}Mg_{0.015})_2(Fe^{2+}_{0.95}Mn^{2+}_{0.05})(Si_2O_7)O[(OH)_{0.58}O_{0.42}]$$

for the RM crystal before and after heating experiments, respectively.

REFERENCES CITED

Amthauer, G., Ghazi-Bayat, G., Lottermoser, W., and Redhammer, G. (1997) Fe^{2+},Fe^{3+}-order, disorder and phase transition in synthetic Al-bearing ilvaites. (abstract). Abstract Supplement 1, Terra Nova, 9, 427.

Bartholomé, P., Duchesne, J.C., and Van der Plas, L. (1968) Sur une forme monoclinique de l'ilvaite. Annales de la Société Geologique de Belgique, 90, 779–788.

Belov, N.V. and Mokeeva, V.I. (1954) The crystal structure of ilvaite. Trudy Instituta Kristallografiya. Akademiya Nauk SSSR, 9, 89–102, (in Russian).

Beran, A. and Bittner, H. (1974) Untersuchungen zur Kristallchemie des Ilvaits. Tschermaks Mineralogische und Petrographische Mitteilungen, 21, 11–29.

Bonazzi, P. and Menchetti, S. (1994) Structural variations induced by heat treatment in allanite and REE-bearing piemontite. American Mineralogist, 79, 1176–1184.

Brown, I.D. and Altermatt, D. (1985) Bond-valence parameters obtained from a systematic analysis of the inorganic crystal structure database. Acta Crystallographica, B41, 244–247.

Burt, D.M. (1971) The facies of some Ca-Fe-Si skarns in Japan. Carnegie Inst. Washington Yearbook, 70, 185–188.

Carrozzini, B. (1994) Crystal structure refinements of ilvaite: new relationships between chemical composition and crystallographic parameters. European Journal of Mineralogy, 6, 465–479.

Dietrich, V. (1972) Ilvait, Ferroantigorit und Greenalith als Begleiter oxidisch-sulfidischer Vererzungen in den Oberhalbsteiner Serpentiniten. Schweizerische Mineralogische und Petrographische Mitteilungen, 52, 57–74.

Evans, B.J. and Amthauer, G. (1980) The electronic structure of ilvaite and the pressure and temperature dependence of its ^{57}Fe Mössbauer spectrum. Journal of Physics and Chemistry of Solids, 41, 985–1001.

Finger, L.W. and Hazen, R.M. (1987) Crystal structure of monoclinic ilvaite and the nature of the monoclinic-orthorhombic transition at high pressure. Zeitschrift für Kristallographie, 179, 415–430.

Finger, L.W., Hazen, R.M., and Hughes, J.M. (1982) Crystal structure of monoclinic ilvaite. Carnegie Inst. Washington Yearbook, 81, 386–388.

Ghazi-Bayat, B., Amthauer, G., Schürmann, K., and Hellner, E. (1987) Synthesis and characterization of the mixed valent iron silicate ilvaite, $CaFe_3[Si_2O_7/O/(OH)]$. Mineralogy and Petrology, 37, 97–108.

Ghazi-Bayat, B., Amthauer, G., and Hellner, E. (1989) Synthesis and characterization of Mn-bearing ilvaite $CaFe^{2+}_{2-x}Mn_xFe^{3+}[Si_2O_7/O/(OH)]$. Mineralogy and Petrology, 40, 101–109.

Ghazi-Bayat, B., Behruzi, M., Litterst, F.J., Lottermoser, W., and Amthauer, G. (1992) Crystallographic phase transition and valence fluctuation in sinthetic Mn-bearing ilvaite $CaFe^{2+}_{2-x}Mn^{2+}_xFe^{3+}[Si_2O_7/O/(OH)]$. Physics and Chemistry of Minerals, 18, 491–496.

Ghazi-Bayat, B., Amthauer, G., and Ahsbahs, H. (1993) High pressure X-ray diffraction study of ilvaite $CaFe^{2+}_2Fe^{3+}[Si_2O_7/O/(OH)]$. Physics and Chemistry of Minerals, 20, 402–406.

Ghose, S. (1969) Crystal chemistry of iron. In K.H. Wedelpohl, Ed., Handbook of Geochemistry, II-3, 26A-10. Springer-Verlag, New York.

———(1988) Charge localization and associated crystallographic and magnetic phase transitions in ilvaite, a mixed-valence iron silicate. In S. Ghose, J.M.D. Coey, and E. Salje, Eds., Structural and Magnetic Phase Transitions in Minerals. Advances in Physical Geochemistry, 7, 141–161. Springer-Verlag, New York.

Ghose, S., Hewat, A.W., Marezio, M., Dang, N.V., Robie, R.A., and Evans, H.T. (1984a) Electron and spin ordering and associated phase transitions in ilvaite, a mixed valence iron silicate. (abstract) Transactions of the American Geophysical Union, 65, 289.

Ghose, S., Hewat, A.W., and Marezio, M. (1984b) A neutron powder diffraction study of the crystal and magnetic structures of ilvaite from 305 K to 5 K—a mixed valence iron silicate with an electronic transition. Physics and Chemistry of Minerals, 11, 67–74.

Ghose, S., Sen Gupta, P.K., and Schlemper, E.O. (1985) Electron ordering in ilvaite, a mixed-valence iron silicate: crystal structure refinement at 138 K. American Mineralogist, 70, 1248–1252.

Ghose, S., Tsukimura, K., and Hatch, D.M. (1989) Phase transitions in ilvaite, a mixed-valence iron silicate. II. A single crystal X-ray diffraction study and Landau theory of the monoclinic to orthorhombic phase transition induced by charge delocalization. Physics and Chemistry of Minerals, 16, 483–496.

Haga, N. and Takéuchi, Y. (1976) Neutron diffraction study of ilvaite. Zeitschrift für Kristallographie, 144, 161–174.

Litterst, F.J. and Amthauer, G. (1984) Electron delocalization in ilvaite, a reinterpretation of its ^{57}Fe Mössbauer spectrum. Physics and Chemistry of Minerals, 10, 250–255.

Naslund, H.R., Hughes, J.M., and Birnie, R.W. (1983) Ilvaite, an alteration product replacing olivine in the Skaergaard intrusion. American Mineralogist, 68, 1004–1008.

Nolet, D.A. and Burns, R.G. (1979) Ilvaite: a study of temperature dependent electron delocalization by the Mössbauer effect. Physics and Chemistry of Minerals, 4, 221–234.

North, A.C.T., Phillips, D.C., and Mathews, F.S. (1968) A semiempirical method of absorption correction. Acta Crystallographica, A24, 351–359.

Phillips, M.W., Popp, R.K., and Clowe, C.A. (1988) Structural adjustments accompanying oxidation-dehydrogenation in amphiboles. American Mineralogist, 73, 500–506.

Phillips, M.W., Draheim, J.E., Popp, R.K., Clowe, C.A., and Pinkerton, A.A. (1989) Effects of oxidation-dehydrogenation in tschermakitic hornblende. American Mineralogist, 74, 764–773.

Robie, R.A., Evans, H.T., Jr., and Hemingway, B.S. (1988) Thermophysical properties of ilvaite $CaFe^{2+}_2 Fe^{3+}Si_2O_7O(OH)$; heat capacity from 7 to 920 K and thermal expansion between 298 and 856 K. Physics and Chemistry of Minerals, 15,

390–397.

Robinson, K., Gibbs, G.V., and Ribbe, P.H. (1971) Quadratic elongation: A quantitative measure of distortion in coordination polyhedra. Science, 172, 567–570

Sheldrick, G.M. (1993) SHELXL-93. A new structure refinement program. University of Gottingen, Germany.

Takéuchi, Y., Haga, N., and Bunno, M. (1983) X-ray study on polymorphism of ilvaite, $HCaFe_2^{2+}Fe^{3+}O_2[Si_2O_7]$. Zeitschrift für Kristallographie, 163, 267–283.

Takéuchi, Y., Sawada, H., and Taniguchi, H. (1993) The ilvaite problem. Proceeding of the Inst. of Natural Sciences, Nihon University, 28, 39–43.

Takéuchi, Y., Sawada, H., Taniguchi, H., Uno, R., and Tabira, Y. (1994) Submicroscopic twinning and chemical inhomogeneity of ilvaite, a mixed-valence iron sorosilicate $HCaFe_2^{2+}Fe^{3+}Si_2O_9$. Zeitschrift für Kristallographie, 209, 861–869.

Xuemin, K., Ghose, S., and Dunlap, B.D. (1988) Phase transition in ilvaite, a mixed-valence iron silicate. I. A ^{57}Fe Mössbauer study of magnetic order and spin frustration. Physics and Chemistry of Minerals, 16, 55–60.

Yamanaka, T. and Takéuchi, Y. (1979) Mössbauer spectra and magnetic features of ilvaites. Physics and Chemistry of Minerals, 4, 149–159.